JACS
JOURNAL OF THE AMERICAN CHEMICAL SOCIETY
pubs.acs.org/JACS
Article

Cooperative Weak Dispersive Interactions Actuate Catalysis in a Shape-Selective Abiological Racemase

Yujia Wang, Michel Rickhaus, Olivier Blacque, Kim K. Baldridge,* Michal Juríček,* and Jay S. Siegel*

Cite This: J. Am. Chem. Soc. 2022, 144, 2679−2684
Read Online
ACCESS | Metrics & More | Article Recommendations | Supporting Information

ABSTRACT: A simple abiological host−guest system demonstrates racemase activity with catalytic rate enhancements of 10^4 without employing traditional functional groups. Cooperative weak interactions enhanced through shape-complementarity between the catalyst active site and the reaction transition state drive this activity, as proposed by Pauling for enzymes. In analogy to the Jencks' concept of catalytic antibodies, it is shown that a hapten resembling the planar transition state of the bowl inversion acts as a potent inhibitor of this catalytic process. In contrast, no substrate/product inhibition is detected, and a relatively weak binding of the substrate is observed ($K_a \approx 10^2$ M^{-1} at 293 K). This simple box-and-bowl system demonstrates that shape selectivity arising from cooperative dispersive forces suffices for the emergence of a catalytic system with an enzyme-like thermodynamic profile.

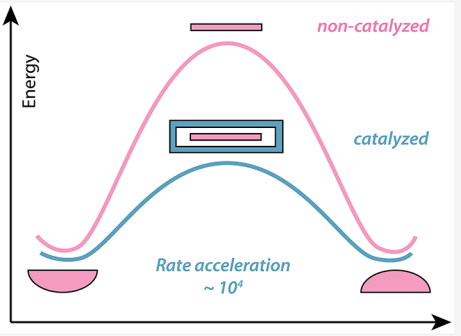

INTRODUCTION

The emergence of biological catalysis most often motivates thoughts of functional groups in specific orientation and propinquity from which the causation between complexity of structure and emergence of function arises.[1] Indeed, catalytic antibodies[2,3] and directed evolution[4] are two sophisticated ways to harness complex biological machinery to create tailored biological catalysts. Despite their complexity, the thermodynamic parameters of these systems can be understood from relatively simple principles outlined by Pauling[5,6] and Jencks,[7] in which the lowering of the overall activation energy of the reaction is associated with either distorting the ground state along the path toward the transition state or stabilizing the transition state by selective binding (Figure 1). Then, can simple abiological systems void of traditional functional groups and accessing only cooperative weak forces, like shape-selective dispersive interactions, suffice to manifest general enzyme profiles with significant rate accelerations?

Catalytic-cavity systems have been reported, but none designed to address the question of a complexity−emergence couple.[8] One such system takes advantage of the remarkable binding affinity of the ExBox cavity for planar polycyclic aromatic hydrocarbons (PAHs), which was parlayed into a modest acceleration of bowl inversion of corannulene (Cor) by exploiting the preferential binding of ExBox to flat vs bowl Cor (Figure 2, top).[9] The reaction was modeled by HDFT methods, and the energetics parsed according to the Pauling−Jencks model. From that work came the idea that a simple abiological system, following the Pauling−Jenks model, could display the characteristics of an enzyme catalyst.

A configurationally stable chiral substrate and a cavity that selectively binds a high-energy achiral form of that substrate could constitute a minimalist abiological racemase. The inverted bowl conformers of monosubstituted corannulenes represent two enantiomers; however, the low-energy barrier for bowl-to-bowl inversion of corannulene (~11.5 kcal mol^{-1}) does not allow their separation. In contrast, peri-annulated

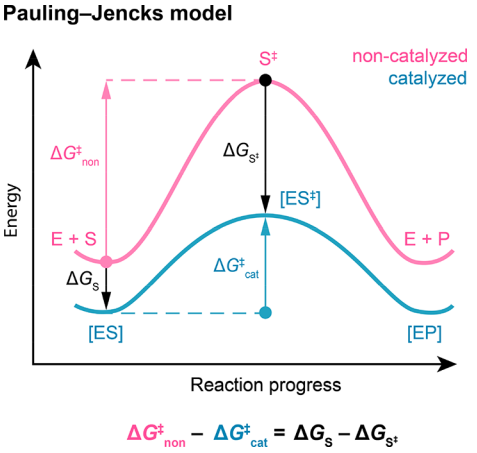

Figure 1. Pauling−Jencks catalysis: Enzyme−substrate binding energy selectively stabilizes the transition state (‡) relative to the ground state. E = enzyme, S = substrate, P = product, [ ] = complex.

Received: October 30, 2021
Published: February 4, 2022

https://doi.org/10.1021/jacs.1c11032
J. Am. Chem. Soc. 2022, 144, 2679−2684

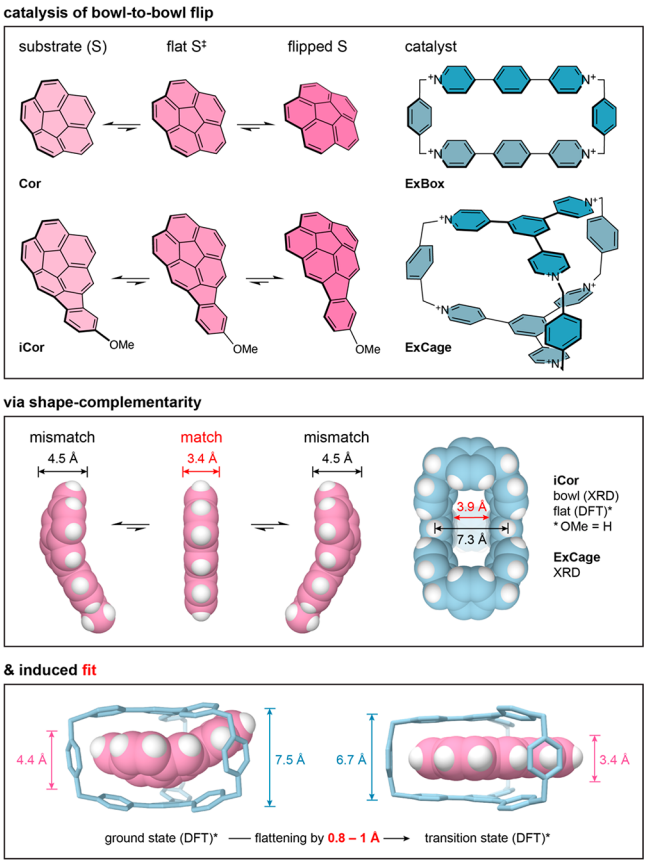

Figure 2. Induced-fit catalysis of a bowl-to-bowl flip. [Top] Substrates, corannulene (Cor) and chiral 2-methoxyindenocorannulene (iCor), that undergo bowl-to-bowl inversion via a planar transition state and the model catalysts, ExBox and ExCage. [Middle] Shape analysis of ExCage cavity dimensions (XRD) with bowl and flat conformation of iCor-H (HDFT). [Bottom] The cavity of ExCage is widened by ∼1 Å when binding bowl vs flat iCor-H (HDFT). iCor-H: OMe = H.

corannulenes show greatly increased barriers for bowl-to-bowl inversion.[10] Specifically, monosubstituted indenocorannulenes exist as resolvable atropisomeric compounds (bowl-inversion barriers >27 kcal mol^{-1}).[10] ExCage has a larger cavity surface and shows higher binding affinity for PAHs than ExBox. Thus, the combination of ExCage (an achiral box)[11] and 2-methoxyindenocorannulene (iCor; a chiral bowl)[10] represents a suitable model for such a highly catalytic abiological racemase (Figure 2, top). This simple box-and-bowl system demonstrates that shape selectivity arising from cooperative dispersive forces suffices for the emergence of a catalytic system with a general enzyme-like thermodynamic and kinetic profile.

RESULTS AND DISCUSSION

For the present study, iCor is the model substrate (Figure 2, top); the bowl inversion process leads to racemization of the enantioenriched sample of iCor, which can be monitored by circular dichroism (CD) spectroscopy. The initial kinetic experiments with ExBox and iCor showed no acceleration of the racemization process (Figure S24), which can be attributed to the binding mode, distinct from that of corannulene, where the corannulene segment of iCor does not fully reside inside the cavity of ExBox but partially protrudes out (Figure S15 and Table S3). Turning attention to the hexacationic bicyclophane ExCage, an analogue of ExBox (Figure 2, top),[12] one sees that the cavity interior (van der Waals radius, r_{vdw}, ≈ 5.5 Å) is large enough to accommodate the corannulene segment (r_{vdw} ≈ 5.3 Å, Figure S1). Contrary to the portal of ExBox (van der Waals distance ∼8.1 Å), the portal of ExCage is narrow yet large enough to accommodate the indeno segment of a bound iCor (Figure 3 and Figure S1).

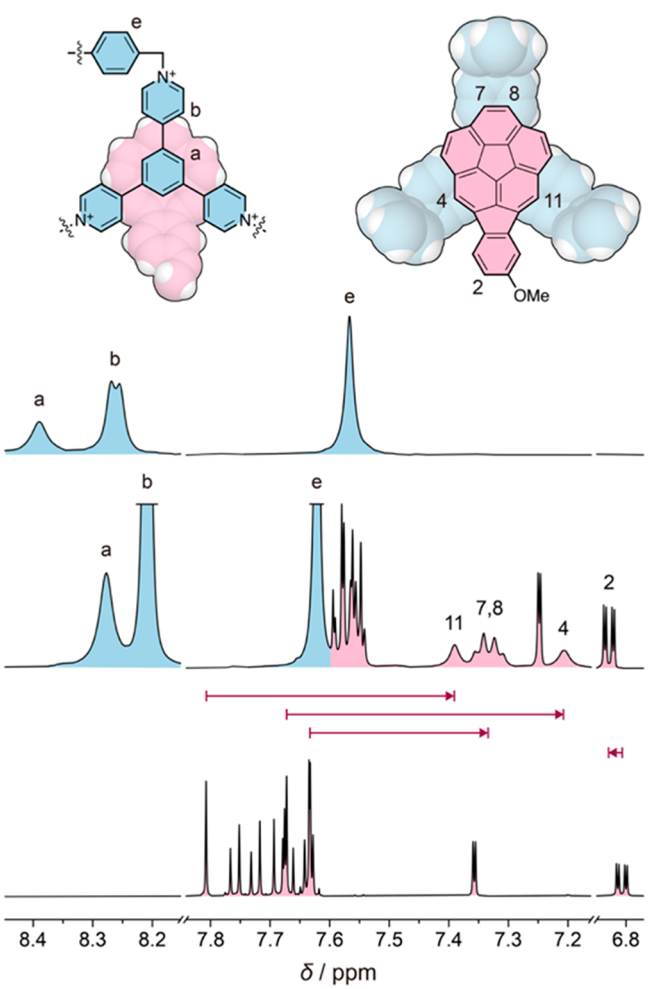

Figure 3. Determination of binding mode via ^{1}H NMR spectroscopy. ^{1}H NMR (600 MHz, CD_3CN) shifts of ExCage (blue, top spectrum) and iCor (pink, bottom spectrum) between unbound species and a 1:1 mixture of ExCage and iCor (middle spectrum, c ≈ 3.3 mM), which indicate the binding mode schematically depicted on top.

The resulting binding mode represents a scenario analogous to ExBox and corannulene, where the corannulene segment of iCor fills up almost the entire interior of ExCage. Because the ground-state bowl conformation of iCor is too thick to fit inside ExCage, both ExCage and iCor undergo "induced-fit" conformational changes,[13,14] as first proposed by Koshland,[15] in order to adjust to the shape mismatch (Figure 2, middle). This structural adjustment, where ExCage widens by ∼0.3 Å (7.27 vs 7.54 Å) and iCor flattens by ∼0.1 Å (4.5 vs 4.4 Å; Figure 2, bottom), results in strain, and widened ExCage can be viewed as an extended tension spring, which forces iCor to adopt a flatter conformation, thereby decreasing the activation energy of the bowl inversion. This situation is analogous to that of molecular compression chambers,[16] in which pushing of

https://doi.org/10.1021/jacs.1c11032
J. Am. Chem. Soc. 2022, 144, 2679−2684

Table 1. Parameters of the ExCage-Catalyzed Bowl-to-Bowl Inversion

substrate	T (K)	K_a (M^{-1})[a]	k_{non} (s^{-1})	k_{obs} (s^{-1})	k_{cat} (s^{-1})	k_{cat}/k_{non}	$\Delta\Delta H^{\ddagger}_{exp}$ (kcal mol^{-1})[f]	$\Delta\Delta H^{\ddagger}_{calc}$ (kcal mol^{-1})[h]
Cor	293	2.4×10^4 ($(3.1 \pm 1.6) \times 10^4$)	6.1×10^3[b]	N/A	6.9×10^5[d]	1.1×10^2	4.4[g]	5.32
iCor	293	1.0×10^2 ($(1.2 \pm 0.6) \times 10^2$)	9.0×10^{-9}	1.4×10^{-5}	2.8×10^{-4}	3.1×10^4	7.8	7.67
iCor	313	65 (73 ± 45)	1.7×10^{-7}	7.4×10^{-5} (1.2×10^{-3})[c]	2.2×10^{-3}	1.3×10^4 (7.1×10^3)[e]	7.8	7.67

[a]The values in parentheses were obtained experimentally from four independent measurements at this temperature, and the values not in parentheses were extrapolated from the Van't Hoff plots shown in Figures S19 (iCor) and S23 (Cor). [b]Calculated using the Eyring equation with $\Delta G^{\ddagger}_{non}$(Cor) = 11.5 kcal mol^{-1} taken from ref 9. [c]With 137 instead of 5 equiv of ExCage. [d]Calculated using the Eyring equation and the $\Delta G^{\ddagger}_{cat}$(Cor) value obtained from the equation $\Delta G^{\ddagger}_{cat} = \Delta G^{\ddagger}_{non} - (\Delta G_S - \Delta G_S^{\ddagger})$, where $\Delta G^{\ddagger}_{non}$(Cor) = 11.5 kcal mol^{-1} was taken from ref 9 and $\Delta G_S^{\ddagger}$ approximated as $\Delta G_S(\text{perylene})_{293} = -9.32$ kcal mol^{-1} was taken from ref 11. [e]Calculated using the k_{obs} value in the parentheses instead of k_{cat}. [f]$\Delta\Delta H^{\ddagger} = \Delta H^{\ddagger}_{non} - \Delta H^{\ddagger}_{cat}$. [g]Calculated using the equation $\Delta\Delta H^{\ddagger} = \Delta H_S - \Delta H_S^{\ddagger}$, where $\Delta H_S^{\ddagger}$ was approximated as ΔH_S(perylene) = −13.1 kcal mol^{-1} taken from ref 11. [h]B97-D/def2-TZVPP (expt solvent).

hydrogen atoms of two opposing Si−H bonds to a distance shorter than the sum of their van der Waals radii leads to a counter-force effect shortening these bonds. Compared to ExBox and corannulene, ExCage[17] and iCor are more rigid, which results in a higher strain upon complexation and, consequently, improvement of the catalytic efficiency in terms of rate enhancement (*vide infra*).

The binding mode and affinity were determined by ^{1}H NMR spectroscopy in CD_3CN. Comparison of the ^{1}H NMR spectra in CD_3CN of unbound iCor and ExCage with that of a 1:1 mixture of iCor and ExCage revealed that iCor resides inside the cavity of ExCage and adopts an orientation shown in Figure 3. In accord with this arrangement, the signals of ExCage protons a and b positioned above the corannulene core are shifted upfield, while the signal of proton e located at the corannulene periphery is shifted downfield. The remaining two ExCage signals positioned in the corners are not affected by the shielding effect of the guest and do not exhibit marked shifts. The same behavior was observed for other aromatic guests.[11] In the case of iCor, all proton signals are shifted upfield except the signal of proton 2, located at the edges of the side phenylene rings of ExCage, which is slightly shifted downfield. The largest shifts are displayed by protons 4 ($\Delta\delta$ ~0.43 ppm), 11 ($\Delta\delta$ ~0.42 ppm), and 7/8 ($\Delta\delta$ ~0.30 ppm), which point toward the side phenylene rings of ExCage perpendicularly to the π-surface.

The binding affinity of ExCage toward iCor was determined by means of variable-temperature (VT) ^{1}H NMR titrations in CD_3CN at a temperature of 258−333 K. A solution of iCor (1.41×10^{-4} M) was titrated with ExCage via a stepwise addition of 1 to 30 equiv at five different temperatures with four independent measurements at each temperature, each with 10 titration points (Figures S16−S18). During titration, the concentration of iCor was kept constant and the concentration of ExCage was in the range $(0-4.23) \times 10^{-3}$ M (see Materials and Methods). The obtained association constants (K_a), ranging from 260 ± 90 M^{-1} at 258 K to 69 ± 82 M^{-1} at 333 K (Table S1), were used to determine the thermodynamic parameters of binding using the Van't Hoff plot: $\Delta H_S = -3.98$ kcal mol^{-1} and $\Delta S_S = -4.42$ cal mol^{-1} K^{-1}. Because of the limited solubility of both components in acetonitrile, the saturation point could not be reached, which accounts for the relatively large standard deviation of the obtained K_a values.

As reported, the binding affinity (K_a) of a planar aromatic guest toward ExCage increases exponentially with the number of π-electrons.[11] If the corannulene segment of iCor were flat, one would expect binding affinity similar to that of perylene ($K_a = 8.9 \times 10^6$ M^{-1} at 293 K and $\Delta H_S = -13.1$ kcal mol^{-1}), which has 20 π-electrons like corannulene. Due to the curved geometry of the corannulene segment, however, the binding affinity of iCor ($K_a \approx 10^2$ M^{-1} at 293 K, Table 1) is lower by almost 5 orders of magnitude than that of perylene. This substantial reduction in binding energy ($\Delta\Delta H \approx 9.1$ kcal mol^{-1}) of iCor toward ExCage is accompanied by structural distortions in both components upon binding, namely, flattening of iCor (by ~0.1 Å; 1.0 vs 1.1 Å) and widening of ExCage (by ~0.3 Å, Figure 2, bottom). In comparison, the energy loss for binding of corannulene inside ExCage (Figure S23) compared to perylene[11] is only about half of that ($\Delta\Delta H \approx 4.4$ kcal mol^{-1}, $\Delta\Delta H$(HDFT) ≈ 5.32 kcal mol^{-1}, Table 1), which is in agreement with the smaller bowl depth (0.87 Å), surface curvature, and inversion barrier of corannulene, compared to iCor, resulting in a closer match to the planar binding affinity.

Having access to enantiomerically enriched iCor,[10] kinetic studies were performed in order to determine the rate enhancement (k_{cat}/k_{non}) of the catalyzed bowl-to-bowl inversion (Table 1), by following the decay of the CD signal. The kinetic measurements were performed in acetonitrile at five different temperatures (333−373 K for iCor and 283−333 K for iCor/**ExCage**), and the rate constants of enantiomerization (k, i.e., k_{cat} and k_{non}) were determined assuming the first-order decay during the early stages of the racemization process ($k = k_{rac}/2$). Because of the relatively low binding affinity of ExCage to iCor and low concentrations that had to be employed during the kinetic measurements on account of limited solubility of iCor in acetonitrile, the majority of iCor (1.1×10^{-4} M) remains unbound even when five equivalents of ExCage (5.5×10^{-4} M) are employed. Therefore, the observed rate constant of enantiomerization (k_{obs}, Table S1) was smaller by approximately 2 orders of magnitude than the "real" rate constant (k_{cat}) of the process occurring inside ExCage. The k_{cat} values were estimated by using the equation $k_{obs} = ak_{cat} + (1 - a)k_{non}$, where a is the percentage of the bound guest determined by using the K_a value. The activation enthalpy ($\Delta H^{\ddagger}$) and entropy ($\Delta S^{\ddagger}$) of enantiomerization were obtained from the Eyring plot and employed in calculating the Gibbs free activation energies at different temperatures by using the equation $\Delta G^{\ddagger}_T = \Delta H^{\ddagger} - T\Delta S^{\ddagger}$. To reinforce the robustness of k_{cat} values coming from this estimation, kinetic measurements with the highest possible concentration of ExCage (1.5×10^{-2} M, 137 equiv) were performed at 283, 313, and 333 K (Table S1). The obtained k_{obs} values ($6.5 \times$

https://doi.org/10.1021/jacs.1c11032
J. Am. Chem. Soc. 2022, 144, 2679−2684

10^{-5} s^{-1} at 283 K, 1.2×10^{-3} s^{-1} at 313 K, and 4.1×10^{-3} s^{-1} at 333 K), representing the lower limit of k_{cat}, are in the same order of magnitude as the k_{cat} values (7.7×10^{-5} s^{-1} at 283 K, 2.2×10^{-3} s^{-1} at 313 K, and 1.5×10^{-2} s^{-1} at 333 K) estimated from the equation above, therefore fully consistent with the extrapolation.

The half-lives of racemization were calculated using the first-order rate constants ($t_{1/2} = \ln 2/k_{rac}$). The racemization of iCor with a half-life of <50 h occurs at temperatures over 60 °C, while the process catalyzed with 5 equiv of ExCage requires temperatures lower by ~50 °C to achieve half-lives comparable to the noncatalyzed process (Table S1). In the temperature range 10−60 °C, the rate enhancement (k_{cat}/k_{non}) is ~10^4 (Table S1 and Figure 4, top), which corresponds to a 7.8 kcal

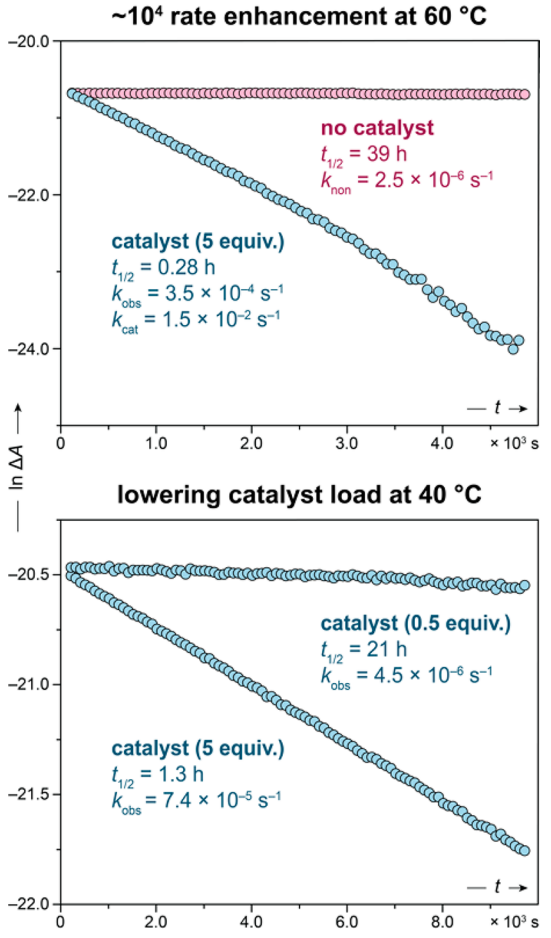

Figure 4. Acceleration of racemization by a catalyst. Following the decay of the CD signal (ln ΔA) in time (t) demonstrates that (top) the bowl-to-bowl inversion is accelerated by a factor of ~10^4 at 60 °C with five equivalents of catalyst and (bottom) a 10-fold decrease of the catalyst load increases the half-life of racemization by a factor of ~20 at 40 °C.

mol^{-1} decrease of $\Delta H^{\ddagger}$. This energy value is in excellent agreement with the HDFT results (7.67 kcal mol^{-1}, Table 1) and close to the value of the "energy loss" of $\Delta\Delta H \approx 9.1$ kcal mol^{-1} in CD_3CN (difference in binding energy of iCor versus perylene inside ExCage) observed upon complexation due to the induced-fit conformational changes. These results demonstrate that perylene represents a good transition-state analogue of iCor (ΔH(perylene) ~ ΔH(iCor‡)) and validates Pauling's concept that the decrease of activation energy is achieved by a greater stabilization of the transition state compared to the ground state:

$$\Delta G^{\ddagger}_{non} - \Delta G^{\ddagger}_{cat} = \Delta G_S - \Delta G^{\ddagger}_S \text{ (Figure 1)}$$

This concept is further illustrated by corannulene, which displays stronger binding as a result of smaller bowl depth and thus smaller shape mismatch, and therefore lower catalytic efficiency (Table 1) in full accord with the above equation (Figure 1).

From the perspective of Koshland's induced fit, the potential energy "stored" in the iCor⊂ExCage complex upon binding effectively decreases the energy barrier for the bowl-to-bowl inversion process and thereby accelerates racemization. This catalytic effect is observed even with substoichiometric amounts of ExCage at 40 °C (Figure 4, bottom, and Figures S38−S42). Notably, racemization at a 7.5% catalyst load at 40 °C occurs with a half-life of ~50 h, despite the relatively low binding affinity of 73 ± 45 M^{-1} (Tables S1 and S2).

To demonstrate further the enzyme-like behavior of our biomimetic system, the Michaelis−Menten plot was attempted, which would allow determination of K_M. Unfortunately, this experiment was not feasible due to solubility limitations.

To illustrate that a "hapten" with a shape reminiscent of the planar transition state can inhibit this catalytic process, kinetic measurements were carried out with phenanthroline in the role of an inhibitor based on the transition-state analogue (Figure 5). Assuming that the binding affinity of ExCage toward

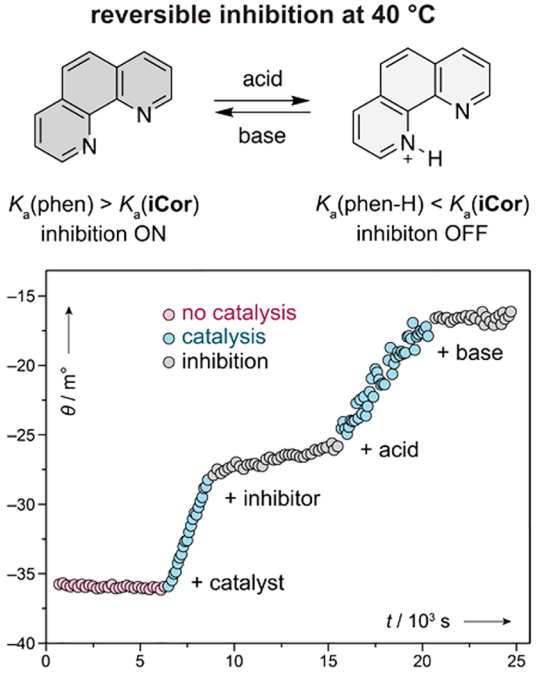

Figure 5. Reversible inhibition of catalysis controlled by pH. The CD signal (θ) of iCor (pink) decays upon the addition of catalyst ExCage (blue). The addition of phenanthroline in the role of inhibitor slows down the decay. Both processes can be reversed by control of pH.

phenanthroline is similar to that of its nonheterocyclic analogue phenanthrene ($K_a = 6.2 \times 10^4$ M^{-1} in acetonitrile at 25 °C) determined previously,[11] phenanthroline should outcompete iCor ($K_a \approx 10^2$ M^{-1} in acetonitrile at 20 °C) in forming a complex with ExCage. Accordingly, the addition of one equivalent of phenanthroline into the solution of a 1:1

https://doi.org/10.1021/jacs.1c11032
J. Am. Chem. Soc. 2022, 144, 2679−2684

mixture of iCor and ExCage substantially slows down the racemization process, as phenanthroline replaces iCor inside the cavity of ExCage. When the pH value is decreased by the addition of acid, phenanthroline is protonated and thus carries a positive charge, which decreases its binding affinity toward hexacationic ExCage. Consequently, iCor replaces the protonated phenanthroline inside the cavity of ExCage and the catalytic racemization process is switched on. Upon the addition of base, neutral phenanthroline is re-formed and replaces iCor inside the cavity of ExCage, thereby turning the inhibition on again and suppressing the catalytic process. This switching behavior is strong evidence that the bowl-to-bowl inversion of iCor, the substrate, is accelerated via formation of an inclusion host−guest complex with ExCage, the catalyst.

CONCLUSION

Abiological racemase activity results from differential dispersion interactions arising from shape complementarity between the substrate/catalyst and transition state/catalyst of the cage-and-bowl system of ExCage and iCor. The organic cage catalyzes racemization of a chiral bowl-shaped hydrocarbon via bowl-to-bowl inversion with a reduction in activation energy of nearly 8 kcal mol^{-1} (a 10^4 rate enhancement). The activation energy of this process is decreased in the greater portion by transition-state stabilization (7 kcal mol^{-1}), augmented by a smaller ground-state destabilization effect (0.7 kcal mol^{-1}). The planar transition state of the substrate is stabilized relative to the ground state through the tailored fitting of the host−guest catalytic complex in accord with Koshland's model of induced fit. The catalytic activity is inhibited by employing a transition-state analogue (phenanthroline) consistent with the Pauling−Jencks model. In contrast, no substrate/product inhibition is seen and a relatively weak binding of the substrate is observed ($K_a \approx 10^2$ M^{-1} at 293 K). This simple abiological system demonstrates the concept and principle of enzyme catalysis using primarily cooperative weak interactions and without the need for an organized array of traditional functional groups.

MATERIALS AND METHODS

NMR Titrations. The ^{1}H NMR (258, 273, 293, 313, 333 K, 500 MHz) titrations were performed by adding small volumes of a stock solution of ExCage·6PF_6 to a solution of iCor or corannulene in MeCN-d_3. The stock solution of ExCage·6PF_6 was prepared using the solution of iCor or corannulene in MeCN-d_3 to keep the concentration of the guest (1.41×10^{-4} M) constant during the titration. The concentration of ExCage was in the range 0 (0 equiv) to 4.23×10^{-3} M (30 equiv). Four independent data sets were used at each temperature to obtain mean values and standard deviations for association constants (K_a). For iCor, the upfield shifts of the ^{1}H resonances for protons 1 (Figure S4a) were observed and used to determine the K_a values, which were obtained using Dynafit,[18] a program that employs nonlinear least-squares regression on host−guest binding data. For corannulene, the ^{1}H resonance could not be observed at each titration point; therefore, only the upfield shifts of the ^{1}H resonances, which were visible and displayed observable shift (labeled with * in Figures S21 and S22), were used to determine the association constants (K_a) by using the equation $\sigma_{ppm(Cor\ obs)} = x\sigma_{ppm(Cor\ bound)} + (1 - x)\sigma_{ppm(Cor\ unbound)}$, where x is the percentage of bound corannulene. The ΔH and ΔS values were obtained through the Van't Hoff plot ($\ln K = \frac{-\Delta H}{RT} + \frac{\Delta S}{R}$).

Kinetic Measurements. Measurements of the rate constants (k) for the bowl-to-bowl inversion of iCor (1.1×10^{-4} M) without and with (5.5×10^{-4} M, 5 equiv) ExCage in acetonitrile were performed by CD time-course measurements at 360 nm, by plotting the decay of absorption against time. The rate constants of enantiomerization (k, i.e., k_{obs}, k_{cat}, or k_{non}) were determined assuming the first-order decay during the early stages of the racemization process ($k = k_{rac}/2$). For iCor, the k_{cat} values were estimated by using the equation $k_{obs} = ak_{cat} + (1 - a)k_{non}$, where a is the percentage of the bound guest determined by using the K_a value. The $\Delta H^{\ddagger}$ and $\Delta S^{\ddagger}$ values were obtained through the Eyring plot ($\ln(k/T)$ against $1/T$) and employed in calculating the Gibbs free activation energies at different temperatures by using the equation $\Delta G^{\ddagger}_T = \Delta H^{\ddagger} - T\Delta S^{\ddagger}$. Kinetic measurements close to or above the boiling point of acetonitrile were carried out in a sealed cuvette.

DFT Calculations. The structural and energetic analyses of the molecular systems for all compounds described in this study were carried out with the B97-D2 dispersion-enabled density functional method (DFT),[19,20] using an ultrafine grid, together with the def2-TZVPP basis set.[21] Full geometry optimizations were performed and uniquely characterized via second derivatives (Hessian) analysis to establish stationary points and effects of zero point and thermal energy contributions. The interaction energies, E_{int}, for formation of complexes from the subunits are defined as $E_{int} = E_{comp} - E_A - E_B$, where E_{comp}, E_A, and E_B are the B97-D/def2-TZVPP(solvent) energy of the complex and energies of the subunits A and B, respectively. Two cases were considered for the interaction energy of complex formation. The first considered all species in their fully relaxed state, and the interaction energy is referred to as $E_{relax.}$ The second case considers the individual subunits in the configuration as adopted within the relaxed complex, referred to as $E_{restrict}$. As such, the difference between E_{relax} and $E_{restrict}$ accounts for effects of geometry change upon complexation. Effects of solvent employed the COSMO:*ab initio* continuum method[22,23] using a dielectric as in experiment and radii of Klamt.[24] Visualization and analysis of structural and property results were obtained using Mercury (e.g., Cor/iCor bowl depth, ExCage cavity dimensions), Avogadro,[25] and GaussView (for spectra).[26] The optimizations and Hessian computations were carried out with G09 ES64L-G09RevE.01.[26]

ASSOCIATED CONTENT

Supporting Information

The Supporting Information is available free of charge at https://pubs.acs.org/doi/10.1021/jacs.1c11032.

NMR, CD, and DFT calculation details (PDF)

Accession Codes

CCDC 2112636 and 2112638 contain the supplementary crystallographic data for this paper. These data can be obtained free of charge via www.ccdc.cam.ac.uk/data_request/cif, or by emailing data_request@ccdc.cam.ac.uk, or by contacting The Cambridge Crystallographic Data Centre, 12 Union Road, Cambridge CB2 1EZ, UK; fax: +44 1223 336033.

AUTHOR INFORMATION

Corresponding Authors

Kim K. Baldridge − *School of Pharmaceutical Science and Technology, Tianjin University, Tianjin 300072, People's Republic of China;* orcid.org/0000-0001-7171-3487; Email: kimbaldridge88@gmail.com

Michal Juríček − *Department of Chemistry, University of Zurich, 8057 Zurich, Switzerland;* orcid.org/0000-0001-5595-431X; Email: michal.juricek@chem.uzh.ch

Jay S. Siegel − *School of Pharmaceutical Science and Technology, Tianjin University, Tianjin 300072, People's Republic of China;* orcid.org/0000-0002-3226-3521; Email: dean_spst@tju.edu.cn

https://doi.org/10.1021/jacs.1c11032
J. Am. Chem. Soc. 2022, 144, 2679−2684

Authors

Yujia Wang − *Department of Chemistry, University of Zurich, 8057 Zurich, Switzerland*

Michel Rickhaus − *Department of Chemistry, University of Zurich, 8057 Zurich, Switzerland;* orcid.org/0000-0002-6107-2310

Olivier Blacque − *Department of Chemistry, University of Zurich, 8057 Zurich, Switzerland*

Complete contact information is available at: https://pubs.acs.org/10.1021/jacs.1c11032

Notes

The authors declare no competing financial interest.

■ ACKNOWLEDGMENTS

This project received funding from the European Research Council (ERC) under the European Union's Horizon 2020 research and innovation program (Grant Agreement No. 716139) and the Swiss National Science Foundation (SNSF, PP00P2_170534 and PP00P2_198900). K.K.B. and J.S.S. are grateful to the National Key Research and Development Program of China (2015CB856500) and NSFC (Grant 21871207).

■ REFERENCES

(1) Bertrán, J. A Darwinian Process: The Molecular Evolution of Enzymes. *Pensamiento* **2008**, *64* (242), 771−782.

(2) Keinan, E. The Enterprise of Catalytic Antibodies: A Historical Perspective. *Catalytic Antibodies*; Wiley-VCH Verlag: Weinheim, 2005.

(3) Kienhöfer, A.; Kast, P.; Hilvert, D. Selective Stabilization of the Chorismate Mutase Transition State by a Positively Charged Hydrogen Bond Donor. *J. Am. Chem. Soc.* **2003**, *125* (11), 3206−3207.

(4) (a) Joyce, G. F. Directed Molecular Evolution. *Sci. Am.* **1992**, *267* (6), 90−99. (b) Arnold, F. H. Directed Evolution Bringing New Chemistry to Life. *Angew. Chem., Int. Ed.* **2018**, *57* (16), 4143−4148.

(5) Pauling, L. Nature of Forces between Large Molecules of Biological Interest. *Nature* **1948**, *161* (4097), 707−709.

(6) Amyes, T. L.; Richard, J. P. Specificity in Transition State Binding: The Pauling Model Revisited. *Biochemistry* **2013**, *52* (12), 2021−2035.

(7) Jencks, W. P. *Catalysis in Chemistry and Enzymology*; McGraw-Hill: New York, 1969.

(8) Lloyd, G.; Forgan, R. S. *Reactivity in Confined Spaces*; R. Soc. Chem.: Croydon, 2021.

(9) Seiders, T. J.; Baldridge, K. K.; Grube, G. H.; Siegel, J. S. Structure/Energy Correlation of Bowl Depth and Inversion Barrier in Corannulene Derivatives: Combined Experimental and Quantum Mechanical Analysis. *J. Am. Chem. Soc.* **2001**, *123* (4), 517−525.

(10) Wang, Y.; Allemann, O.; Balaban, T. S.; Vanthuyne, N.; Linden, A.; Baldridge, K. K.; Siegel, J. S. Chiral Atropisomeric Indenocorannulene Bowls: Critique of the Cahn−Ingold−Prelog Conception of Molecular Chirality. *Angew. Chem., Int. Ed.* **2018**, *57* (22), 6470−6474.

(11) Dale, E. J.; Vermeulen, N. A.; Thomas, A. A.; Barnes, J. C.; Juríček, M.; Blackburn, A. K.; Strutt, N. L.; Sarjeant, A. A.; Stern, C. L.; Denmark, S. E.; Stoddart, J. F. ExCage. *J. Am. Chem. Soc.* **2014**, *136* (30), 10669−10682.

(12) Barnes, J. C.; Juríček, M.; Strutt, N. L.; Frasconi, M.; Sampath, S.; Giesener, M. A.; McGrier, P. L.; Bruns, C. J.; Stern, C. L.; Sarjeant, A. A.; Stoddart, J. F. ExBox: A Polycyclic Aromatic Hydrocarbon Scavenger. *J. Am. Chem. Soc.* **2013**, *135* (1), 183−192.

(13) Juríček, M.; Strutt, N. L.; Barnes, J. C.; Butterfield, A. M.; Dale, E. J.; Baldridge, K. K.; Stoddart, J. F.; Siegel, J. S. Induced-Fit Catalysis of Corannulene Bowl-to-Bowl Inversion. *Nat. Chem.* **2014**, *6* (3), 222−228.

(14) Ibáñez, S.; Peris, E. Dimensional Matching versus Induced-Fit Distortions: Binding Affinities of Planar and Curved Polyaromatic Hydrocarbons with a Tetragold Metallorectangle. *Angew. Chem., Int. Ed.* **2020**, *59* (17), 6860−6865.

(15) Koshland, D. E. Correlation of Structure an Function in Enzyme Action. *Science* **1963**, *142* (3599), 1533−1541.

(16) Baldridge, K. K.; Siegel, J. S. Molecular Compression Chambers: Exceeding the Euler Modulus. *J. Phys. Org. Chem.* **2015**, *28* (3), 223−225.

(17) ExCage with a higher binding affinity for PAHs is also a better catalyst for the corannulene inversion (10^2 acceleration) compared to ExBox, primarily as a result of the greater transition-state stabilization as seen in the context of the Pauling−Jencks model.

(18) Kuzmic, P. Program DYNAFIT for the Analysis of Enzyme Kinetic Data: Application to HIV Proteinase. *Anal. Biochem.* **1996**, *237* (2), 260−273.

(19) Grimme, S. Semiempirical GGA-Type Density Functional Constructed with a Long-Range Dispersion Correction. *J. Comput. Chem.* **2006**, *27* (15), 1787−1799.

(20) Grimme, S. Semiempirical Hybrid Density Functional with Perturbative Second-Order Correlation. *J. Chem. Phys.* **2006**, *124* (3), 34108.

(21) Weigend, F.; Ahlrichs, R. Balanced Basis Sets of Split Valence Triple Zeta Valence and Quadruple Zeta Valence Quality for H to Rn: Design and Assessment of Accuracy. *Phys. Chem. Chem. Phys.* **2005**, *7* (18), 3297−3305.

(22) Klamt, A.; Schüürmann, G. COSMO: A New Approach to Dielectric Screening in Solvents with Explicit Expressions for the Screening Energy and Its Gradient. *J. Chem. Soc., Perkin Trans.* **1993**, *2* (5), 799−805.

(23) Baldridge, K.; Klamt, A. First Principles Implementation of Solvent Effects without Outlying Charge Error. *J. Chem. Phys.* **1997**, *106* (16), 6622−6633.

(24) Klamt, A.; Jonas, V.; Bürger, T.; Lohrenz, J. C. W. Refinement and Parametrization of COSMO-RS. *J. Phys. Chem. A* **1998**, *102* (26), 5074−5085.

(25) Hanwell, M. D.; Curtis, D. E.; Lonie, D. C.; Vandermeersch, T.; Zurek, E.; Hutchison, G. R. Avogadro: An Advanced Semantic Chemical Editor, Visualization, and Analysis Platform. *J. Cheminform.* **2012**, *4* (1), 17.

(26) Frisch, M. J.; Trucks, G. W.; Schlegel, H. B.; Scuseria, G. E.; Robb, M. A.; Cheeseman, J. R.; Scalmani, G.; Barone, V.; Mennucci, B.; Petersson, G. A.; Nakatsuji, H.; Caricato, M.; Li, X.; Hratchian, H. P.; Izmaylov, A. F.; Bloino, J.; Zheng, G.; Sonnenberg, J. L.; Hada, M.; Ehara, M.; Toyota, K.; Fukuda, R.; Hasegawa, J.; Ishida, M.; Nakajima, T.; Honda, Y.; Kitao, O.; Nakai, H.; Vreven, T.; Montgomery, J. A., Jr.; Peralta, J. E.; Ogliaro, F.; Bearpark, M.; Heyd, J. J.; Brothers, E.; Kudin, K. N.; Staroverov, V. N.; Keith, T.; Kobayashi, R.; Normand, J.; Raghavachari, K.; Rendell, A.; Burant, J. C.; Iyengar, S. S.; Tomasi, J.; Cossi, M.; Rega, N.; Millam, J. M.; Klene, M.; Knox, J. E.; Cross, J. B.; Bakken, V.; Adamo, C.; Jaramillo, J.; Gomperts, R.; Stratmann, R. E.; Yazyev, O.; Austin, A. J.; Cammi, R.; Pomelli, C.; Ochterski, J. W.; Martin, R. L.; Morokuma, K.; Zakrzewski, V. G.; Voth, G. A.; Salvador, P.; Dannenberg, J. J.; Dapprich, S.; Daniels, A. D.; Farkas, O.; Foresman, J. B.; Ortiz, J. V.; Cioslowski, J.; Fox, D. J. *Gaussian 09*, Revision E.01; Gaussian, Inc.: Wallingford, CT, 2013.